Acta Mech 223, 2021–2038 (2012)
DOI 10.1007/s00707-012-0691-3

C. Jiang · X. Han · G. Y. Lu

A hybrid reliability model for structures with truncated probability distributions

Received: 14 March 2011 / Revised: 17 May 2012 / Published online: 24 June 2012

Abstract In traditional reliability analysis, the uncertain parameters are generally treated by some ideal probability distributions with infinite tails, which, however, seems inconsistent with the practical situations as nearly all the uncertain parameters in engineering structures will get their values within a limited interval. To eliminate such an inconsistence and thereby improve the precision of the reliability analysis, the truncated probability distributions are then employed to quantify the uncertainty in this paper, and a corresponding reliability analysis method is developed. Two cases of positional relations are summarized for the uncertainty domain and the failure surface according to whether their intersection set is non-empty or empty. The probability and non-probability convex model methods are employed to deal with these two cases, respectively, and based on it, a hybrid reliability model is then constructed for truncated distribution problems. An efficient approach is also provided to distinguish these two positional relations and thereby determine which one of the probability and non-probability methods should be used when computing a real hybrid reliability. Five numerical examples are investigated to demonstrate the effectiveness of the present method.

1 Introduction

Traditional reliability analysis techniques are in general based on probability and statistical theory, in which the uncertain parameters are treated as random distributions and the failure probability of the structure needs to be evaluated. Presently, the probability model has become a principal means of conducting the reliability analysis for structures under uncertainty and been successfully applied to varieties of industrial departments. Many practical methods in this field have been well established, which include the first-order reliability method (FORM) [1–3], second-order reliability method (SORM) [4–6], system reliability analysis [7,8], Monte Carlo-based simulation method [9,10], reliability-based optimization design [11–17]. In the above-mentioned methods, the involved parameters are generally quantified by some kinds of ideal probability distributions, such as normal, lognormal, exponential, Weibull, etc. Most of these distributions have two infinite tails (such as normal distribution) or only one infinite tail (such as exponential distribution). However, in practical engineering problems, nearly all the random parameters will take their values within a bounded range. An example is that the dimensions of a product actually belong to some intervals formed by the nominal values and the manufacturing tolerances like 10 ± 0.01 mm. We can refer to such a probability distribution as *truncated distribution*. If the truncating points are far from the means of the uncertain parameters, consequences caused

C. Jiang · X. Han (✉) · G. Y. Lu
State Key Laboratory of Advanced Design and Manufacturing for Vehicle Body,
College of Mechanical and Vehicle Engineering, Hunan University, Changsha 410082, People's Republic of China
E-mail: hanxu@hnu.edu.cn
Tel.: +86-731-8823993
Fax: +86-731-8821445

C. Jiang
E-mail: jiangchaoem@yahoo.com.cn

by the truncation are often insignificant. However, as the parameters' intervals become tighter, the influences brought by the truncation can no longer be ignored [18]. In such cases, using the ideal probability distributions to deal with the uncertain parameters will inevitably result in a relatively large error of the reliability analysis. To improve the reliability analysis precision, it seems more reasonable and also promising to use the truncated distributions to deal with the uncertain parameters existing in the structure.

Perhaps because using the ideal probability distributions can make the reliability analysis very convenient, and furthermore such a treatment may be sufficiently precise for some practical applications, presently there has been remarkably little discussion about the reliability analysis for truncated distributions in the literature. Sun and He deduced the doubly truncated *probability density functions* (PDFs) for several commonly used random distributions and furthermore gave an analytic form to compute the reliability for linear limit-state functions [19]. He and Wang [20] adopted a singly truncated distribution to describe the resistance force and formulated a method to calculate the structural reliability index. Xu and Chen [21] proposed a kind of Monte Carlo simulation method for structural reliability analysis with truncated distributions. Melchers et al. [22] proposed a modified FORM algorithm to deal with the structural reliability problem with discontinuous and truncated PDFs. Based on the construction of a statistical model using truncated distributions, Sweet and Tu [18] presented a new approach to evaluate the tolerances of the fit between a bore and a shaft. In the above-mentioned works, the traditional reliability methods for ideal probability distributions were just taken to evaluate the reliability for truncated distribution problems nearly without any changes. However, it should be noted that actually these two kinds of reliability problems are quite different. For a truncated distribution problem, the uncertainty domain forms a multidimensional box with limited bounds, which will lead to two different cases of positional relations between the uncertainty domain and the failure surface. In the first case, the uncertainty domain has a non-empty intersection set with the failure surface, and the traditional methods developed for ideal distributions can still work well. In the second one, the uncertainty domain is completely separated from the failure surface, and if the traditional reliability methods are used to deal with the failure surfaces falling into this case, we will obtain an exactly same reliability equal to 1.0 or 0.0. In other words, the traditional methods will lose effectiveness as they can no longer distinguish which one is most reliable among these failure surfaces. What is more, it will in general lead to a numerical difficulty of convergence to use the traditional methods to deal with a truncated distribution problem, especially when the second case of positional relation emerges [22].

Mathematically, the bound uncertainty will be involved in a truncated probability distribution problem, which is just the origin resulting in the above difficulties. Actually, the bound uncertainty can be treated through a new kind of uncertainty analysis technique called *convex model*. In the convex model, the uncertain parameters are treated as a multidimensional ellipsoid or interval variables. It was firstly proposed and explored by Ben-Haim and Elishakoff [23] since entering the 1990s and further developed by many other researchers in the past two decades [24–29]. A parameter perturbation method was proposed to compute the dynamic response bounds for structures with interval uncertain parameters [24]. A robust design method was developed for structures by using convex model to deal with the uncertainty [25]. By using a satisfaction degree of interval to deal with the uncertain constraints, a convex-model-based optimization method was developed for structures [26]. A new method was presented to obtain the confidence structural responses of truss structures under ellipsoid static load uncertainty [27]. An optimization method was developed via a convex model superposition technique, in which one layer of optimization process was successfully eliminated and a high computational efficiency was achieved [28]. The optimal design of structural systems was investigated for structures subjected to uncertainties in the load magnitudes and in the resistance of the members [29].

Concentrating on the above problems, this paper aims to develop a new reliability analysis method for structures with truncated probability distributions by introducing the convex model method. The remainder of this paper is organized as follows. First, the truncated distribution and corresponding reliability problem are given in Sect. 2. Second, a new hybrid reliability model is proposed to deal with the truncated distribution problems in Sect. 3. Third, five numerical examples are investigated to demonstrate the effectiveness of the present method in Sect. 4. Finally, the conclusion is summarized in Sect. 5.

2 Reliability analysis by using truncated probability distributions

2.1 Truncated probability distribution

As shown in Fig. 1, for an ideal probability distribution with a PDF $f_X(x)$, its doubly truncated PDF $\bar{f}_X(x)$ can be defined by [30]:

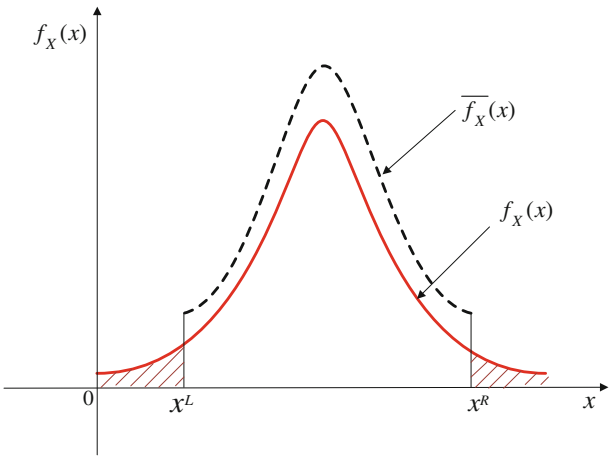

Fig. 1 A doubly truncated PDF

$$\bar{f}_X(x) = \begin{cases} m \cdot f_X(x), & x^L \le x \le x^R \\ 0, & \text{otherwise} \end{cases} \tag{1}$$

where x^L and x^R denote the lower and upper truncating bounds, respectively. The coefficient m can be computed by

$$m = \frac{1}{\int_{-\infty}^{x^R} f_X(x)\mathrm{d}x - \int_{-\infty}^{x^L} f_X(x)\mathrm{d}x} = \frac{1}{F_X(x^R) - F_X(x^L)} \tag{2}$$

where F_X stands for the cumulative distribution function (CDF). Thus, the CDF of the truncated distribution can be defined by

$$\bar{F}_X(x) = \begin{cases} 0, & x < x^L, \\ \frac{F_X(x) - F_X(x^L)}{F_X(x^R) - F_X(x^L)}, & x^L \le x < x^R, \\ 1, & x^R \le x. \end{cases} \tag{3}$$

For a truncated distribution, the determination of the truncating points is a very important issue. Theoretically, these points should be specified through precise experimental measurements. However, in practical applications, many of them can be easily obtained through some theoretical analysis methods or just our engineering experience. For example, the interval of a dimension parameter can be determined through its nominal value and the machining tolerance. Another example is that for most of the engineering materials two standard deviations off from the midpoint can be used as the truncating points of their strength and yield limits [30]. For convenience of analysis, in this paper we adopt a theoretical analysis method, namely the *equal CDF method* [21], to determine the truncating points, in which the cut CDF parts at the two ends should be guaranteed to be the same:

$$F_X(x^L) = 1 - F_X(x^R) = C_F \tag{4}$$

where $0 \le C_F < 0.5$ stands for the truncating ratio of CDF. Substituting Eq. (4) into Eqs. (1) and (3) results in the following:

$$\bar{f}_X(x) = \begin{cases} \frac{f_X(x)}{1-2C_F}, & x^L \le x \le x^R \\ 0, & \text{otherwise} \end{cases}, \quad \bar{F}_X(x) = \begin{cases} 0, & x < x^L, \\ \frac{F_X(x) - C_F}{1-2C_F}, & x^L \le x < x^R, \\ 1, & x^R \le x. \end{cases} \tag{5}$$

Based on Eq. (4), x^L and x^R can be analytically determined for some commonly used distributions such as:

(i) Normal distribution

$$x^L = \phi^{-1}(C_F)\sigma + \mu, \quad x^R = \phi^{-1}(1 - C_F)\sigma + \mu \tag{6}$$

where μ and σ denote the expected value and standard deviation, respectively; ϕ^{-1} denotes an inverse CDF of the standard normal distribution.

(ii) Lognormal distribution

$$\begin{aligned} x^L &= \exp\left(\sqrt{\ln\left(1+\left(\frac{\sigma}{\mu}\right)^2\right)}\phi^{-1}(C_F) + \ln\left(\mu \Big/ \sqrt{1+\left(\frac{\sigma}{\mu}\right)^2}\right)\right), \\ x^R &= \exp\left(\sqrt{\ln\left(1+\left(\frac{\sigma}{\mu}\right)^2\right)}\phi^{-1}(1 - C_F) + \ln\left(\mu \Big/ \sqrt{1+\left(\frac{\sigma}{\mu}\right)^2}\right)\right). \end{aligned} \tag{7}$$

(iii) Type I extreme value

$$x^L = -\ln(-\ln(C_F))/a + b, \quad x^R = -\ln(-\ln(1 - C_F))/a + b, \tag{8}$$

where a and b are two distribution parameters in the Type I extreme value CDF.

(iv) Exponential distribution (only has the upper truncating bound)

$$x^R = -\mu \ln(C_F). \tag{9}$$

2.2 Reliability analysis problem

For a structure subjected to uncertainty, based on the traditional probability analysis its reliability R can be defined:

$$R = \Pr\{g(\mathbf{X}) \geq 0\}, \tag{10}$$

where Pr represents the probability and g denotes a limit-state function where the structure is safe if $g(\mathbf{X}) \geq 0$. The equation $g(\mathbf{X}) = 0$ is usually called the *failure surface*. $\mathbf{X}$ is an n-dimensional vector of independent random variables, which herein are all truncated probability distributions with the following variation intervals:

$$x_i \in x_i^I = \left[x_i^L, x_i^R\right], \quad x_i^c = \frac{x_i^L + x_i^R}{2}, \quad i = 1, 2, \ldots, n, \tag{11}$$

where x_i^c denotes the midpoint of the ith interval. Like most of the structural analysis, here $g(\mathbf{X}^c)$ is assumed to be larger than 0, which is usually true in practical engineering problems as a real structure is in general safe at its nominal design. The reliability R can be computed by the following integral:

$$R = \Pr\{g(\mathbf{X}) \geq 0\} = \int\limits_{g(\mathbf{X})\geq 0} \bar{f}_{\mathbf{X}}(\mathbf{X})\mathrm{d}\mathbf{X}, \tag{12}$$

where $\bar{f}_{\mathbf{X}}(\mathbf{X})$ denotes the joint PDF of the truncated random variables.

For a reliability problem with truncated distributions, the uncertainty domain will form a multidimensional box instead of an infinite or semi-infinite space, and the joint PDF $\bar{f}_{\mathbf{X}}(\mathbf{X})$ takes non-zero values only within this box. According to whether the uncertainty domain intersects with the failure surface, different types of positional relations will emerge. As will be indicated in the following Section, the traditional probability methods are only applicable to some cases of positional relations, while lose effectiveness for the other ones. Thus, a new reliability model with wider applicability should be developed for the above truncated distribution problems.

3 A new reliability analysis method for truncated distribution problems

As shown in Fig. 2, we can summarize all the possible positional relations between the uncertainty domain and the failure surface into two different types. In our method, different approaches will be suggested to evaluate the reliability for the two types of positional relations, and based on it, a hybrid reliability model will be subsequently proposed for structures with truncated distributions.

3.1 Reliability analysis for the first type of positional relation

In this case, the uncertainty domain and the failure surface have a non-empty intersection set like the two failure surfaces g_1 and g_2 in Fig. 2. If the probability methods to evaluate the reliability are used, the integration field in Eq. (12) will be formed by the uncertainty domain and the failure surface. For different failure surfaces, we will then have different sizes and shapes of integration fields and hence different probability values. Namely, the obtained probability can well reflect the reliability of each failure surface, and hence in this case, the traditional probability methods are still suggested for computation of the structural reliability.

Due to its simplicity and high efficiency, the well-known FORM is used here, in which the original random variables $\mathbf{X}$ (in x space) should be firstly transformed into a set of standard normal variables $\mathbf{U}$ (in u space) [31]:

$$\phi(u_i) = \bar{F}_{X_i}(x_i), \quad u_i = \phi^{-1}\left[\bar{F}_{X_i}(x_i)\right], \quad i = 1, 2, \ldots, n \tag{13}$$

where $\bar{F}_{X_i}$ denotes the CDF of the ith truncated random variable. A corresponding limit-state function G in u space can be obtained:

$$g(\mathbf{X}) = g(T(\mathbf{U})) = G(\mathbf{U}), \tag{14}$$

where T denotes a probability transformation function based on Eq. (13). Then, the integration in Eq. (12) can be rewritten as:

$$R = \Pr\{g(\mathbf{X}) \geq 0\} = \int_{G(\mathbf{U})\geq 0} f_{\mathbf{U}}(\mathbf{U})\mathrm{d}\mathbf{U}, \tag{15}$$

where $f_{\mathbf{U}}$ denotes a joint CDF of the standard normal variables $\mathbf{U}$. The following optimization problem can be created to compute the reliability index β of the structure:

$$\begin{cases} \beta = \min_{\mathbf{U}} \|\mathbf{U}\|, \\ \text{s.t. } G(\mathbf{U}) = 0, \end{cases} \tag{16}$$

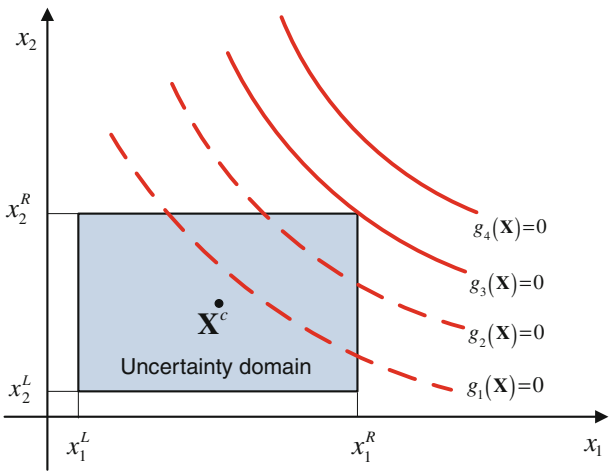

Fig. 2 Positional relation between the uncertainty domain and the failure surface

where $\|\cdot\|$ denotes the quadratic norm of a vector. The optimum $\mathbf{U}^*$ is called the *most probable point* (MPP), and the reliability index $\beta = \|\mathbf{U}^*\|$ represents a minimum distance from the origin to the failure surface in u space. Finally, the reliability R in Eq. (15) can be approximately obtained:

$$R \approx \phi(\beta) = \phi\left(\|\mathbf{U}^*\|\right). \tag{17}$$

The efficient HL-RF algorithm [1,2] is adopted to solve the optimization problem in Eq. (16), which can be formulated by the following iterations:

$$\begin{aligned} \beta^k &= \frac{G(\mathbf{U}^k) - \left(\nabla G(\mathbf{U}^k)\right)^T \mathbf{U}^k}{\|\nabla G(\mathbf{U}^k)\|}, \\ \mathbf{U}^{k+1} &= -\beta^k \frac{\nabla G(\mathbf{U}^k)}{\|\nabla G(\mathbf{U}^k)\|}, \end{aligned} \tag{18}$$

where ∇G denotes the gradient vector of G with respect to the random variables.

3.2 Reliability analysis for the second type of positional relation

In this case, there exists an empty intersection set between the failure surface and the uncertainty domain like g_3 and g_4 in Fig. 2. If the traditional probability methods are used to evaluate the reliability, we will always obtain an identical reliability value equal to 1.0 for all the failure surfaces belonging to this case. That is to say, based on the probability analysis, these failure surfaces should be regarded to have an exactly same reliability, which, however, seems inconsistent with the practical situations. For example, in a practical engineering problem, a failure surface like g_4 is obviously more reliable than g_3, because it has a further distance to the uncertainty domain than the latter and thereby has a smaller possibility to fail. However, the probability analysis cannot grasp this important characteristic, as here an exactly same probability reliability will be achieved for g_3 and g_4. Furthermore, by using the probability reliability methods to deal with a truncated distribution problem, a numerical difficulty of convergence is likely to be encountered [22]. To overcome the above difficulties, in our formulation a non-probability convex model technique [32] is extended to perform the reliability analysis when the second type of positional relation emerges.

By conducting a non-probability analysis, the uncertainty of all the parameters should be quantified only through their variation intervals x_i^I, $i = 1, 2, \ldots, n$, and a corresponding limit-state function can be created:

$$g\left(x_1^I, x_2^I, \ldots, x_n^I\right). \tag{19}$$

It should be noted that the non-probability intervals here are actually quite different from the above truncated probability distributions though they have two exactly same bounds for each parameter. The non-probability interval only contains the bound information of an uncertain parameter, while the truncated distribution has not only the bound information but also the probability information over the interval.

Then, all the intervals need to be normalized:

$$x_i^I = x_i^c + x_i^r \delta_i, \quad i = 1, 2, \ldots, n \tag{20}$$

where $x_i^r = (x_i^R - x_i^L)/2$ denotes the radius of the ith interval, and the normalized variables δ_i, $i = 1, 2, \ldots, n$ are confined in a symmetric convex polyhedron $C_\delta = \{\boldsymbol{\delta} | \delta_i \in [-1, 1], i = 1, 2, \ldots, n\}$. Thus, the origin point of the normalized space just corresponds to the midpoint $\mathbf{X}^c$ of the parameters.

Substituting Eq. (20) into Eq. (19) will result in a new limit-state function G' in the normalized space:

$$g\left(x_1^I, x_2^I, \ldots, x_n^I\right) = G'\left(\delta_1, \delta_2, \ldots, \delta_n\right). \tag{21}$$

After extending the normalized space $C_\delta = \{\boldsymbol{\delta} | \delta_i \in [-1, 1], i = 1, 2, \ldots, n\}$ to a corresponding infinite space $C_\delta^\infty = \{\boldsymbol{\delta} | \delta_i \in [-\infty, \infty], i = 1, 2, \ldots, n\}$, a *non-probability reliability index* of the structure can be defined as the minimum distance from the origin to the normalized failure surface $G' = 0$ [32,33]. Then, the following optimization problem can be created to compute the non-probability reliability index η:

$$\begin{cases} \eta = \min\limits_{\boldsymbol{\delta}} \{\|\boldsymbol{\delta}\|_\infty\} = \min\limits_{\boldsymbol{\delta}} \{\max\left(|\delta_1|, |\delta_2|, \ldots, |\delta_n|\right)\} \\ \text{s.t. } G'(\boldsymbol{\delta}) = 0 \end{cases} \tag{22}$$

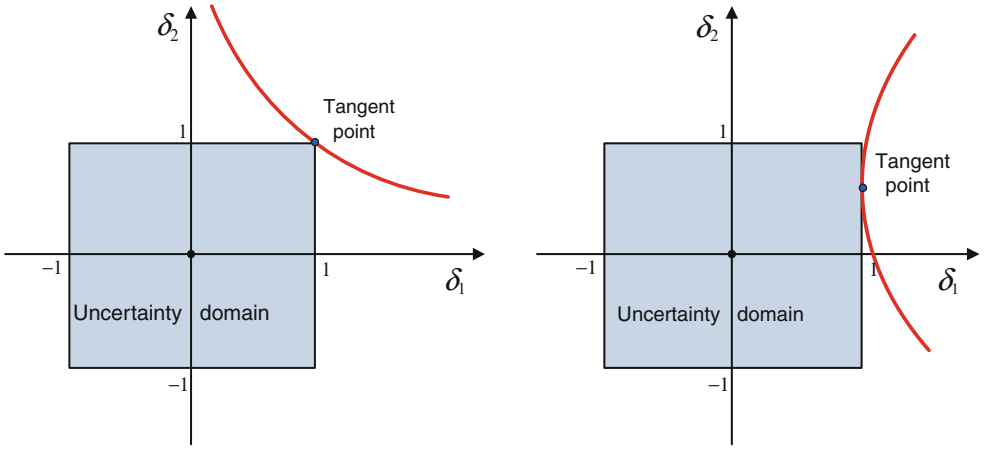

Fig. 3 Cases of $\eta = 1$ in the normalized space

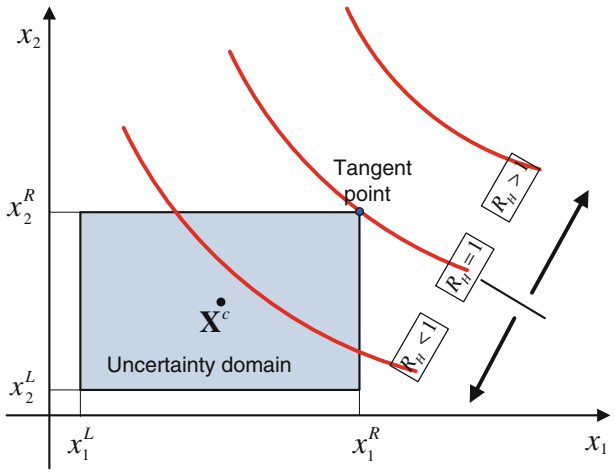

Fig. 4 Variation pattern of the hybrid reliability

where $\|\cdot\|_\infty$ denotes the infinite norm of a vector. In this paper, the sequential quadratic programming (SQP) [34] is used to search the optimum $\boldsymbol{\delta}^*$ of the above optimization problem.

Geometrically, $\eta = 1$ implies that the uncertainty domain is tangent to the failure surface, that is to say, they have only one intersection point as shown in Fig. 3. $\eta > 1$ means a desirable reliability for the structure as the uncertainty domain is always inside the reliable field. Additionally, as the failure surface moves away from the uncertainty domain, the structure will obviously become more reliable, and correspondingly the η will also become larger. Therefore, through the above non-probability analysis technique, the structural reliability under the second type of positional relation can be clearly described.

3.3 A hybrid reliability model

Synthesizing the above two cases, a hybrid reliability R_H can then be constructed to deal with the reliability problems with truncated probability distributions:

$$R_H = \begin{cases} R = \phi(\beta) = \phi(\|\mathbf{U}^*\|), & \left\{\mathbf{X}|\, x_i^L \le x_i \le x_i^R, i = 1, 2, \ldots, n\right\} \cap \{\mathbf{X}|\, g(\mathbf{X}) = 0\} \neq \emptyset, \\ \eta = \left\|\boldsymbol{\delta}^*\right\|_\infty, & \left\{\mathbf{X}|\, x_i^L \le x_i \le x_i^R, i = 1, 2, \ldots, n\right\} \cap \{\mathbf{X}|\, g(\mathbf{X}) = 0\} = \emptyset, \end{cases} \tag{23}$$

where $\{\mathbf{X}|x_i^L \le x_i \le x_i^R, i = 1, 2, \ldots, n\}$ and $\{\mathbf{X}|g(\mathbf{X}) = 0\}$ denote the uncertainty domain and the failure surface, respectively.

As shown in Fig. 4, when the uncertainty domain and the failure surface have a non-empty intersection set, the hybrid reliability R_H will be equivalent to the traditional probability reliability R, and we have $R_H \le 1$.

On the contrary, if the intersection set is empty, the hybrid reliability will be equivalent to the non-probability reliability index η, and we have $R_H > 1$. An inflexion point occurs when the uncertainty domain is tangent to the failure surface, and we have $R_H = 1$.

As indicated in Eq. (23), whether the uncertainty domain intersects with the failure surface needs to be judged when computing the hybrid reliability R_H, which is not an easy job in practical applications. The following procedure can be adopted as a simple treatment to this problem:

(i) Use the non-probability analysis method in Sect. 3.2 to compute the reliability index η.
(ii) If $\eta > 1$, it can be sure that there exists an empty intersection set between the uncertainty domain and the failure surface, and we have $R_H = \eta$.
(iii) If $\eta \leq 1$, it can sure that the intersection set is non-empty, and the probability analysis method in Sect. 3.1 should be used to compute the reliability R again and we then have $R_H = R$.

Obviously, the above approach is very stable and applicable to general problems. However, it is not an efficient method, because we need to carry out both the probability and non-probability analysis for a hybrid reliability when $\eta \leq 1$.

To improve the efficiency, here we provide another approach to compute the hybrid reliability, in which a vertex point of the multidimensional uncertainty box is selected to judge whether the uncertainty domain intersects with the failure surface, instead of a time-consuming non-probability analysis process. Two preconditions should be satisfied for this approach. The first one is $g(\mathbf{X}^c) > 0$, which we have mentioned that will generally hold true. The other one is that the limit-state function should be ensured to be monotonic over the uncertainty domain; in other words, a very strong non-linearity is not allowed for the limit-state function. For most practical engineering problems, this precondition is also not hard to satisfy, as the uncertainty of a structural parameter always behaves as a small disturbance around its nominal value, and hence the whole uncertainty domain will be relatively narrow. Thus, it seems not difficult to keep the monotonicity for a practical limit-state function over such a small domain. The approach then can be outlined as follows:

(i) Compute the gradient $\frac{\partial G'(\boldsymbol{\delta})}{\partial \delta_i}|_{\boldsymbol{\delta}=0}$ of the limit-state function with respect to the ith uncertain parameter at the midpoint $\boldsymbol{\delta} = 0$.
(ii) If $\frac{\partial G'(\boldsymbol{\delta})}{\partial \delta_i}|_{\boldsymbol{\delta}=0} < 0$, based on the above two preconditions, it can be qualitatively predicted that the failure surface in δ space will locate on the positive part of the coordinate axis. In other words, if an intersection point exists between the failure surface and the δ_i axis, it should have a positive value of δ_i. In this case, make $Y_i = X_i^R$.
(iii) If $\frac{\partial G'(\boldsymbol{\delta})}{\partial \delta_i}|_{\boldsymbol{\delta}=0} > 0$, it can be predicted that the failure surface will locate on the negative part of the coordinate axis and in this case make $Y_i = X_i^L$.
(iv) Repeat the above steps for all the uncertain parameters, and an n-dimensional vector $\mathbf{Y}$ can be finally achieved, which actually stores a vertex point of the multidimensional uncertainty box.
(v) Compute the value of $g(\mathbf{Y})$. If $g(\mathbf{Y}) > 0$, it is sure that the uncertainty domain and the failure surface have an empty intersection set, and the non-probability analysis method should be used to compute the hybrid reliability. On the contrary, $g(\mathbf{Y}) \leq 0$ implies a non-empty intersection set, and correspondingly the probability analysis method should be used to compute the hybrid reliability.

In the above analysis, a vertex point $\mathbf{Y}$ is selected as a judge point to distinguish the positional relation of the uncertainty domain and the failure surface. Among all the 2^n vertex points of the uncertainty box, $\mathbf{Y}$ has the closest distance to the failure surface. As shown in Fig. 5, a two-dimensional problem is taken as an example to illustrate the use of the suggested approach. If the gradients $\frac{\partial G'(\boldsymbol{\delta})}{\partial \delta_1}|_{\boldsymbol{\delta}=0}$ and $\frac{\partial G'(\boldsymbol{\delta})}{\partial \delta_2}|_{\boldsymbol{\delta}=0}$ are both smaller than 0, we will have a failure surface with the shape and location like g_1 and g_2, and according to our method, the vertex point in the upper right corner should be used as the judge point $\mathbf{Y}$, which obviously has a smaller distance to the failure surface than the other three ones. Then, for a failure surface with no intersection set with the uncertainty domain like g_2, we have $g(\mathbf{Y}) > 0$. Otherwise, we have $g(\mathbf{Y}) \leq 0$ for a failure surface like g_1. By using the above approach, we can easily judge whether the uncertainty domain intersects with the failure surface only through a very small number of functional evaluations, and hence, a high computational efficiency can be ensured for the hybrid reliability analysis. On the other hand, as $\frac{\partial g(\boldsymbol{X})}{\partial X_i}|_{\mathbf{X}=\mathbf{X}^c}$ and $\frac{\partial G'(\boldsymbol{\delta})}{\partial \delta_i}|_{\boldsymbol{\delta}=0}$ has an exactly same sign, they can be both used in the above procedure.

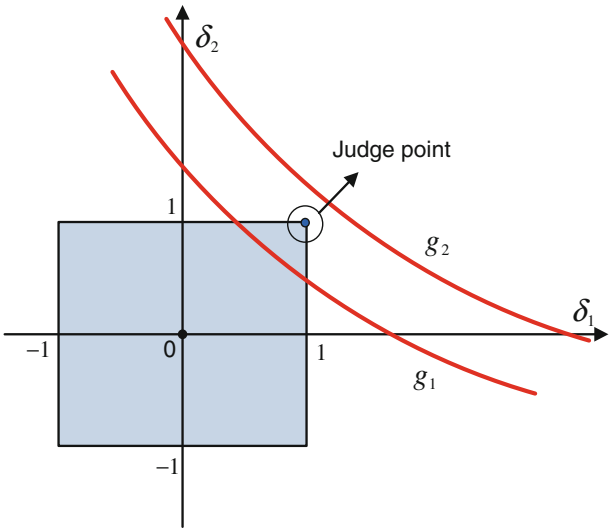

Fig. 5 Judgment of the positional relation by using a vertex point

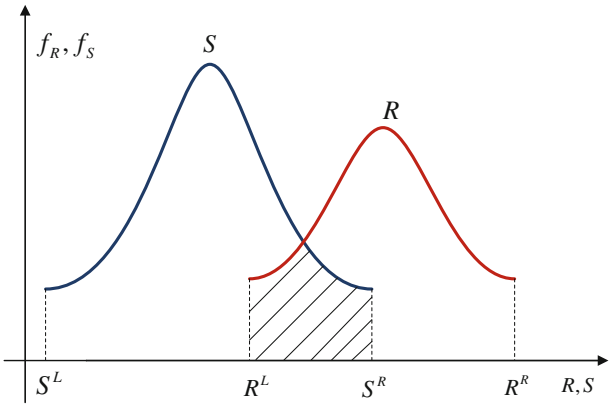

Fig. 6 A stress–strength model for structural reliability analysis

4 Numerical examples and discussion

Five numerical examples will be investigated, among which three are simple problems with explicit expressions and the other two are based on simulation models. For convenience of the analysis, the equal CDF method is employed to determine the truncating points, and furthermore, the truncating ratios of all the concerned parameters in each numerical example are given a same value C_F.

4.1 A traditional stress–strength model

As shown in Fig. 6, a traditional stress–strength model for structural reliability analysis is considered. The strength R and stress S are both truncated normal distributions, and their ideal distribution parameters are $\mu_R = 500$ Mpa, $\sigma_R = 50$ Mpa, $\mu_S = 400$ Mpa and $\sigma_S = 80$ Mpa. A limit-state function is given by:

$$g(R, S) = R - S. \tag{24}$$

Due to the linear limit-state function, the hybrid reliability can be analytically computed. When $R^L \leq S^R$, the probability method should be used to calculate the hybrid reliability:

$$R_H = \Pr(R - S > 0) = \int_{S^L}^{R^L} \bar{f}_S(S)\mathrm{d}S + \int_{R^L}^{S^R} \bar{f}_S(S) \left[\int_{S}^{R^R} \bar{f}_R(R)\mathrm{d}R \right] \mathrm{d}S, \tag{25}$$

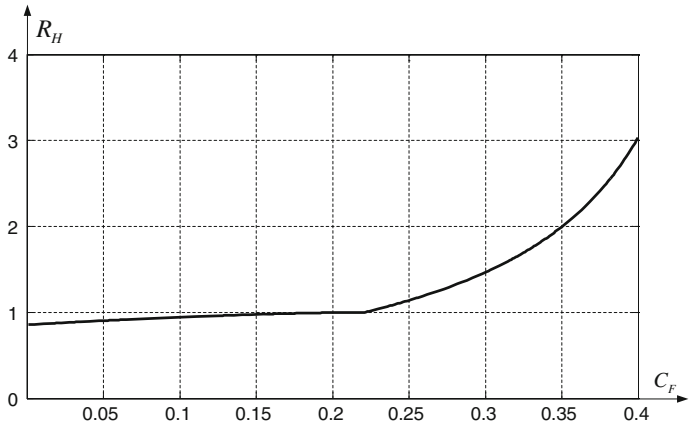

Fig. 7 Variation of the hybrid reliability with respect to the truncating ratio for the stress–strength problem

Table 1 Hybrid reliabilities of the stress–strength problem under several cases of C_F

C_F	0.00	0.10	0.20	0.22	0.30	0.35	0.40
R_H	0.855	0.944	0.997	1.000	1.466	2.067	3.032

where the truncated PDFs $\bar{f}_S$ and $\bar{f}_R$ can be given by:

$$\begin{aligned} \bar{f}_R(R) &= \frac{f_R(R)}{1-2C_F} = \frac{1}{(1-2C_F)\sqrt{2\pi}\sigma_R}\exp\left(-\frac{(R-\mu_R)^2}{2\sigma_R^2}\right), \\ \bar{f}_S(S) &= \frac{f_S(S)}{1-2C_F} = \frac{1}{(1-2C_F)\sqrt{2\pi}\sigma_S}\exp\left(-\frac{(S-\mu_S)^2}{2\sigma_S^2}\right). \end{aligned} \tag{26}$$

Substituting Eq. (26) into Eq. (25) results in

$$\begin{aligned} R_H = {} & \frac{1}{1-2C_F}\left(\phi\left(\frac{R^L-\mu_S}{\sigma_S}\right)-\phi\left(\frac{S^L-\mu_S}{\sigma_S}\right)\right) \\ & +\frac{1}{(1-2C_F)^2}\phi\left(\frac{R^R-\mu_R}{\sigma_R}\right)\left(\phi\left(\frac{S_R-\mu_S}{\sigma_S}\right)-\phi\left(\frac{R^L-\mu_S}{\sigma_S}\right)\right) \\ & -\frac{1}{(1-2C_F)^2}\int_{R^L}^{S^R}\frac{1}{\sqrt{2\pi}}\exp\left(-\frac{(S-\mu)^2}{2\sigma_S^2}\right)\phi\left(\frac{S-\mu_R}{\sigma_R}\right)\mathrm{d}S. \end{aligned} \tag{27}$$

When $R^L > S^R$, the non-probability method should be used to calculate the hybrid reliability. The two parameter intervals need to be transformed into the normalized space:

$$R^I = R^c + R^r\delta_R, \quad S^I = S^c + S^r\delta_S. \tag{28}$$

Then, a limit-state function in the normalized space can be created:

$$G'(R,S) = R^r\delta_R - S^r\delta_S + (R^c - S^c) = 0. \tag{29}$$

It is also a linear function, and hence, the non-probability reliability index can be explicitly obtained:

$$R_H = \frac{R^c - S^c}{R^r + S^r}. \tag{30}$$

Making the truncating ratio C_F change continuously within the interval [0, 0.4] and for each C_F, the hybrid reliability is computed by the above formulas. A variation curve then can be obtained as shown in Fig. 7, and the hybrid reliabilities under some specific truncating ratios are also provided in Table 1. It can be found

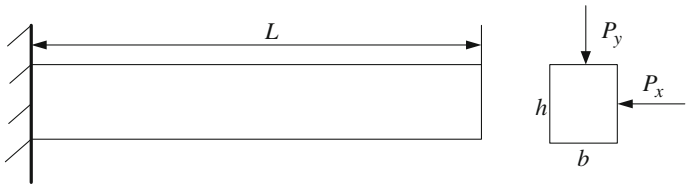

Fig. 8 A cantilever beam [35]

that the hybrid reliability behaves as a continuous and monotonically increasing variation with respect to the truncating ratio C_F. It is because that with increase in the truncating ratio the uncertainty domain will become narrower. Therefore, the relative distance between the uncertainty domain and the failure surface will become larger, which makes the structure have a smaller possibility to fail and thereby a better reliability. Additionally, the variation curve can be divided into two different stages according to its rate of change, and the inflexion point occurs at $C_F = 0.22$ where the hybrid reliability is just equal to 1. In the first stage, the hybrid reliability increases from 0.855 to 1 with nearly a constant speed when the truncating ratio C_F changes from 0 to 0.22, and in this stage, the probability analysis method is used. In the second stage, the non-probability analysis method is used, and the hybrid reliability changes with an increasing speed. For $C_F = 0.4$, the reliability reaches to a large value 3.032.

4.2 A cantilever beam

As shown in Fig. 8, a cantilever beam modified from the numerical example in reference [35] is investigated. Considering that the maximum stress at the fixed end of the beam should be less than a yield strength $S = 320$ Mpa, a limit-state function can be created as follows:

$$g\left(b, h, P_x, P_y\right) = S - \frac{6P_xL}{b^2h} - \frac{6P_yL}{bh^2}, \tag{31}$$

where $L = 1$ m is the length of the beam; b and h stand for the width and height of the cross section, respectively; and P_x and P_y stand for the horizontal force and vertical force, respectively. In this problem, b and h both follow the truncated normal distribution, and their ideal distribution parameters are $\mu_b = 0.1$ m, $\sigma_b = 0.01$ m, $\mu_h = 0.2$ m and $\sigma_h = 0.015$ m; P_x and P_y both follow the truncated lognormal distribution, and their ideal distribution parameters are $\mu_{P_x} = 65{,}000$ N, $\sigma_{P_x} = 7{,}800$ N, $\mu_{P_y} = 40{,}000$ N and $\sigma_{P_y} = 2{,}400$ N.

We also make the truncating ratio C_F vary within an interval $[0, 0.41]$ and use the present method to compute the hybrid reliability at each specific C_F. In the analysis process, the following gradients are required:

$$\begin{aligned}
&\left.\frac{\partial g(\mathbf{X})}{\partial b}\right|_{\mathbf{X}=\mathbf{X}^c} = \frac{12P_xL}{b^3h} + \frac{6P_yL}{b^2h^2} > 0, \quad \left.\frac{\partial g(\mathbf{X})}{\partial h}\right|_{\mathbf{X}=\mathbf{X}^c} = \frac{12P_yL}{bh^3} + \frac{6P_xL}{b^2h^2} > 0,\\
&\left.\frac{\partial g(\mathbf{X})}{\partial P_x}\right|_{\mathbf{X}=\mathbf{X}^c} = \frac{-6L}{b^2h} < 0, \quad \left.\frac{\partial g(\mathbf{X})}{\partial P_y}\right|_{\mathbf{X}=\mathbf{X}^c} = \frac{-6L}{bh^2} < 0.
\end{aligned} \tag{32}$$

It can be found that the first two gradients are always larger than 0, while the second two are always smaller than 0. Thus, for all the different C_F, a same vertex point (b^L, h^L, P_x^R, P_y^R) is used to judge whether the uncertainty domain and the failure surface have an intersection set. Collecting all the computational results, a variation curve of the hybrid reliability can then be achieved, as shown in Fig. 9. Additionally, the hybrid reliabilities at seven specific truncating ratios are also given in Table 2. It can be found that the obtained variation curve has a similar shape as the one in the first numerical example, which is continuous and monotonically increasing with respect to the truncating ratio C_F. Also, the variation curve consists of two segments. In the first one, the hybrid reliability is a nearly linear function of the truncating ratio, while in the second one it behaves with a certain degree of non-linearity. The inflexion point of the hybrid reliability occurs at $C_F = 0.27$.

4.3 A 10-bar truss

As shown in Fig. 10, a 10-bar truss [27–29] is considered. The Young's modulus E of the truss is 68,948 Mpa and the density ρ is 2, 768 Kg/m^3. The length L of the horizontal and vertical bars is 9.144m. A vertical force

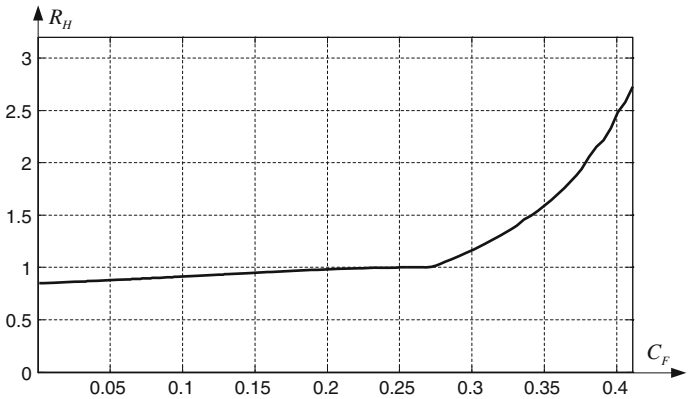

Fig. 9 Variation of the hybrid reliability with respect to the truncating ratio for the cantilever beam

Table 2 Hybrid reliabilities of the cantilever beam under several cases of C_F

C_F	0.00	0.10	0.20	0.27	0.30	0.35	0.41
R_H	0.848	0.913	0.981	1.000	1.170	1.599	2.726

F_1 is applied on the node 4, and a vertical force F_2 and a horizontal force F_3 are applied on the node 2. The cross-sectional areas $A_i, i = 1, 2, \ldots, 10$ of the bars are random variables all following the truncated normal distribution, and they have the same distribution parameters $\mu_A = 6.5 \times 10^{-3}\,\mathrm{m}^2$ and $\sigma_A = 3.25 \times 10^{-4}\,\mathrm{m}^2$. The vertical displacement d_y of the node 2 needs to be less than a maximum value $d_a = 2.7 \times 10^{-2}\,\mathrm{m}$, and hence, a following limit-state function can be created:

$$g(\mathbf{A}) = d_a - d_y(\mathbf{A}). \tag{33}$$

The axial forces $N_j, j = 1, 2, \ldots, 10$ in the bars can be computed by [25]:

$$\begin{cases} N_1 = F_2 - \frac{\sqrt{2}}{2}N_8, \quad N_2 = -\frac{\sqrt{2}}{2}N_{10}, \\ N_3 = -F_1 - 2F_2 + F_3 - \frac{\sqrt{2}}{2}N_8, \quad N_4 = -F_2 + F_3 - \frac{\sqrt{2}}{2}N_{10}, \\ N_5 = -F_2 - \frac{\sqrt{2}}{2}N_8 - \frac{\sqrt{2}}{2}N_{10}, \quad N_6 = -\frac{\sqrt{2}}{2}N_{10}, \\ N_7 = \sqrt{2}\,(F_1 + F_2) + N_8, \quad N_8 = \frac{a_{22}b_1 - a_{12}b_2}{a_{11}a_{22} - a_{12}a_{21}}, \\ N_9 = \sqrt{2}F_2 + N_{10}, \quad N_{10} = \frac{a_{11}b_2 - a_{21}b_1}{a_{11}a_{22} - a_{12}a_{21}} \end{cases} \tag{34}$$

where

$$\begin{cases} a_{11} = \left(\frac{1}{A_1} + \frac{1}{A_3} + \frac{1}{A_5} + \frac{2\sqrt{2}}{A_7} + \frac{2\sqrt{2}}{A_8}\right)\frac{L}{2E}, \\ a_{12} = a_{21} = \frac{L}{2A_5E}, \\ a_{22} = \left(\frac{1}{A_2} + \frac{1}{A_4} + \frac{1}{A_6} + \frac{2\sqrt{2}}{A_9} + \frac{2\sqrt{2}}{A_{10}}\right)\frac{L}{2E}, \\ b_1 = \left(\frac{F_2}{A_1} - \frac{F_1 + 2F_2 - F_3}{A_3} - \frac{F_2}{A_5} - \frac{2\sqrt{2}(F_1 + F_2)}{A_7}\right)\frac{\sqrt{2}L}{2E}, \\ b_2 = \left(\frac{\sqrt{2}(F_3 - F_2)}{A_4} - \frac{\sqrt{2}F_2}{A_5} - \frac{4F_2}{A_9}\right)\frac{L}{2E}. \end{cases} \tag{35}$$

The maximum displacement d_y is then computed by:

$$d_y = \left(\sum_{i=1}^{6}\frac{N_i^0 N_i}{A_i} + \sqrt{2}\sum_{i=7}^{10}\frac{N_i^0 N_i}{A_i}\right)\frac{L}{E}, \tag{36}$$

where N_i^0 can be calculated through Eq. (34) with a substitution $F_1 = F_3 = 0$ and $F_2 = 1$.

Like the preceding two numerical examples, here the truncating ratio C_F is also changed within an interval $[0, 0.445]$. By using the present method to compute the hybrid reliability, the gradients of the limit-state

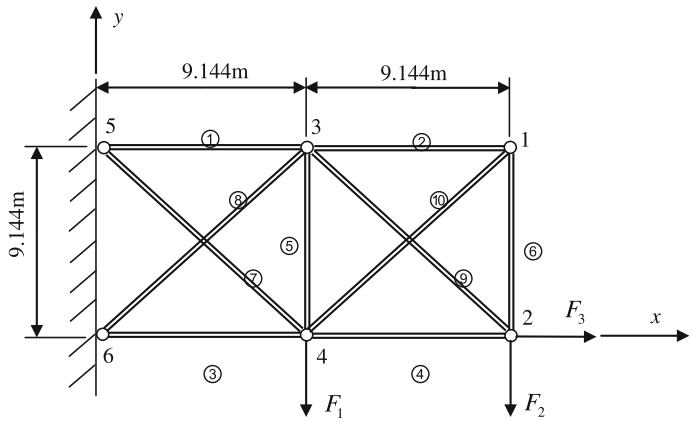

Fig. 10 A 10-bar truss [29]

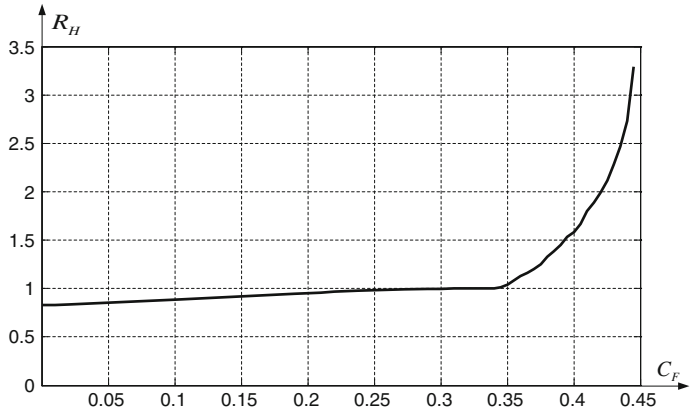

Fig. 11 Variation of the hybrid reliability with respect to the truncating ratio for the 10-bar truss

Table 3 Hybrid reliabilities of the 10-bar truss under several cases of C_F

C_F	0.00	0.10	0.20	0.30	0.345	0.40	0.445
R_H	0.827	0.885	0.952	0.998	1.000	1.584	3.291

function with respect to the uncertain parameters are required, and in this example, they always satisfy the following inequalities:

$$\begin{aligned}
&\left.\frac{\partial g(\mathbf{A})}{\partial A_1}\right|_{\mathbf{A}=\mathbf{A}^c} > 0, \quad \left.\frac{\partial g(\mathbf{A})}{\partial A_2}\right|_{\mathbf{A}=\mathbf{A}^c} > 0, \quad \left.\frac{\partial g(\mathbf{A})}{\partial A_3}\right|_{\mathbf{A}=\mathbf{A}^c} < 0,\\
&\left.\frac{\partial g(\mathbf{A})}{\partial A_4}\right|_{\mathbf{A}=\mathbf{A}^c} < 0, \quad \left.\frac{\partial g(\mathbf{A})}{\partial A_5}\right|_{\mathbf{A}=\mathbf{A}^c} > 0, \quad \left.\frac{\partial g(\mathbf{A})}{\partial A_6}\right|_{\mathbf{A}=\mathbf{A}^c} > 0,\\
&\left.\frac{\partial g(\mathbf{A})}{\partial A_7}\right|_{\mathbf{A}=\mathbf{A}^c} > 0, \quad \left.\frac{\partial g(\mathbf{A})}{\partial A_8}\right|_{\mathbf{A}=\mathbf{A}^c} > 0, \quad \left.\frac{\partial g(\mathbf{A})}{\partial A_9}\right|_{\mathbf{A}=\mathbf{A}^c} > 0, \quad \left.\frac{\partial g(\mathbf{A})}{\partial A_{10}}\right|_{\mathbf{A}=\mathbf{A}^c} > 0.
\end{aligned} \tag{37}$$

Thus, the same vertex point $(A_1^L, A_2^L, A_3^R, A_4^R, A_5^L, A_6^L, A_7^L, A_8^L, A_9^L, A_{10}^L)$ is used as the judge point when computing the hybrid reliability for each truncating ratio. A variation curve of the hybrid reliability is given in Fig. 11, and the hybrid reliabilities at seven specific truncating ratios are also provided in Table 3. When C_F changes from 0 to 0.345, the hybrid reliability can be found slowly increasing from 0.827 to 1, while rapidly rising from 1 to 3.291 when C_F changes from 0.345 to 0.445. The inflexion point of the probability and non-probability analysis occurs at $C_F = 0.345$.

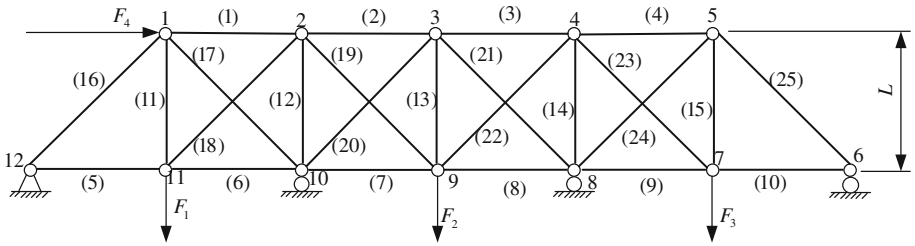

Fig. 12 A 25-bar truss [28]

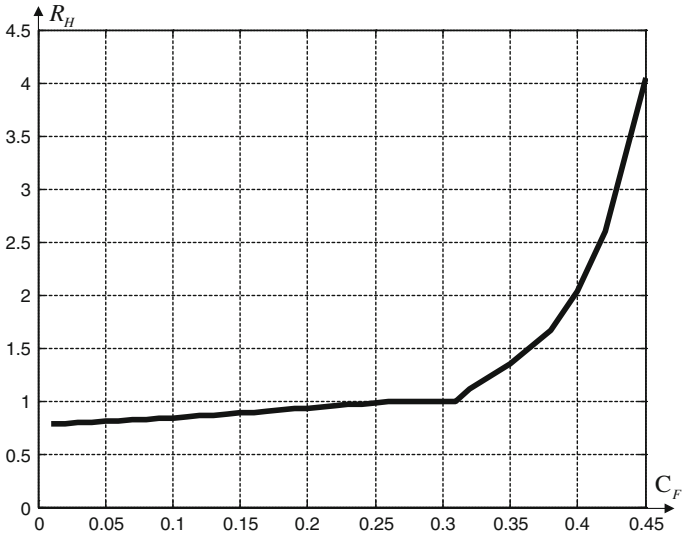

Fig. 13 Variation of the hybrid reliability with respect to the truncating ratio for the 25-bar truss

Table 4 Hybrid reliabilities of the 25-bar truss under several cases of C_F

C_F	0.00	0.10	0.20	0.31	0.35	0.40	0.45
R_H	0.778	0.842	0.932	1.000	1.343	2.029	4.043

4.4 A 25-bar truss

A 25-bar truss as shown in Fig. 12 is considered. This structure as well as some other trusses has been well studied in the references [28,29]. Young's modulus E of the truss is 199,949.2 MPa, and Poisson's ratio ν is 0.3. The length L of each horizontal or vertical bar is 15.24 m. Joint 12 is hinge-supported, and joints 6, 8 and 10 are roller-supported. Joints 7, 9 and 11 are subjected to the vertical loads $F_3 = 1,779.2$ KN, $F_2 = 2,224$ KN and $F_1 = 1,779.2$ KN, respectively. Joint 1 is subjected to a horizontal load $F_4 = 1,334.4$ KN. The bars (1)–(4) have a same cross-sectional area denoted by A_1, the bars (5)–(10) A_2, the bars (11)–(15) A_3, the bars (16) and (17) A_4, the bars (18) and (19) A_5, the bars (20) and (21) A_6, the bars (22) and (23) A_7, and the bars (24) and (25) A_8. All the above areas follow the truncated normal distribution, and their ideal distribution parameters are $\mu_{A_1} = 600\,\text{mm}^2$, $\sigma_{A_1} = 60\,\text{mm}^2$, $\mu_{A_2} = 8{,}000\,\text{mm}^2$, $\sigma_{A_2} = 800\,\text{mm}^2$, $\mu_{A_3} = 6{,}000\,\text{mm}^2$, $\sigma_{A_3} = 600\,\text{mm}^2$, $\mu_{A_4} = \mu_{A_5} = \mu_{A_6} = \mu_{A_7} = \mu_{A_8} = 5{,}000\,\text{mm}^2$ and $\sigma_{A_4} = \sigma_{A_5} = \sigma_{A_6} = \sigma_{A_7} = \sigma_{A_8} = 500\,\text{mm}^2$, respectively. Considering that the vertical displacement δ of joint 9 should be less than an allowable value 36 mm, a limit-state function can be created as follows:

$$g(\mathbf{A}) = 36\,\text{mm} - \delta(\mathbf{A}). \tag{38}$$

The finite element method (FEM) is used to calculate the structural displacement response δ. The truss element is employed to create the FEM mesh. Each bar is an element, and there are a total of 25 elements.

By using the present method, a variation curve of the hybrid reliability is obtained as shown in Fig. 13, and Table 4 gives its values at some specific truncating ratios. It can be found that the hybrid reliability first

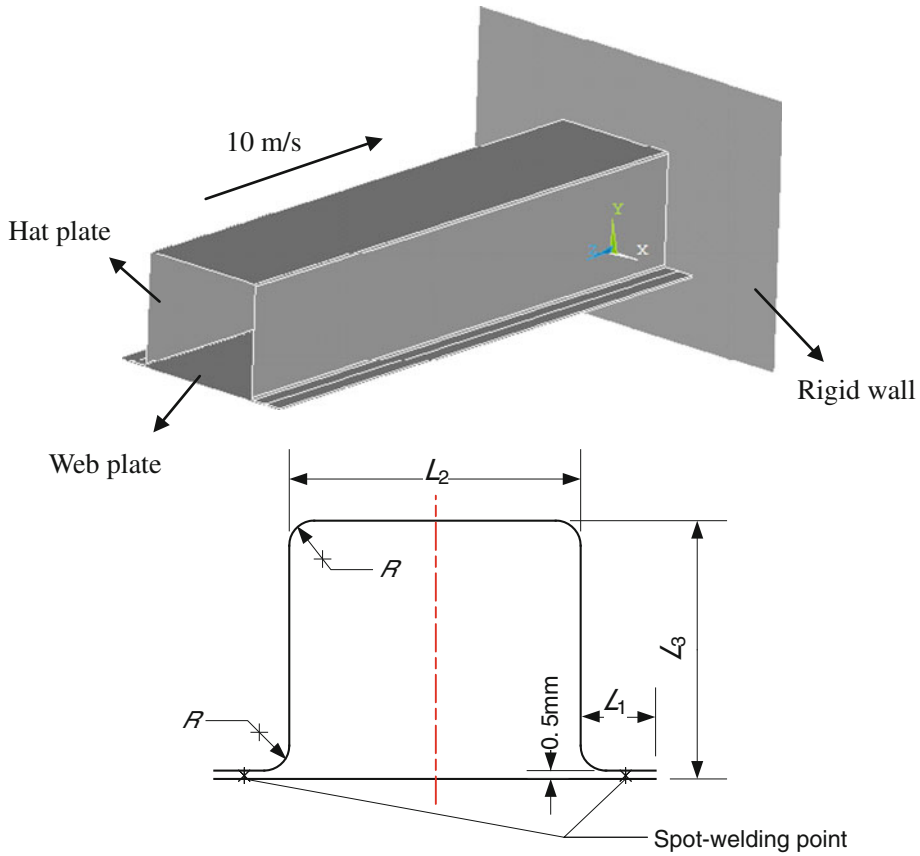

Fig. 14 A closed-hat beam impacting a rigid wall and its cross section [36]

slowly increases from 0.778 to 1 when C_F varies from 0 to 0.31, while it rapidly rises from 1 to 4.043 when C_F changes from 0.31 to 0.45. The inflexion point occurs at $C_F = 0.31$.

4.5 An engineering application

The thin-walled beams connected by spot welding are major structures of an automotive body for load support and energy absorption [36]. The crashworthiness performance is a very important consideration for the design of thin-walled beams. As shown in Fig. 14, a closed-hat beam impacting a rigid wall with an initial velocity 10 m/s is investigated in this application, which is a kind of typical thin-walled beam in practical automotive bodies. It is formed by a hat beam and a web plate, which are connected by some uniformly distributed spot-welding points along the two rims of the hat beam. Due to the manufacturing and measuring deviations, the dimensions L_1, L_2 and L_3, the plate thickness t and round radius R are treated as random parameters. Because their values will not exceed some limited bounds in practical situations, here the truncating distributions are employed to quantify the deviations of these five uncertain parameters. Among them, L_1, L_2 and L_3 all follow the truncated normal distribution, and their ideal distribution parameters are $\mu_{L_1} = 18$ mm, $\sigma_{L_1} = 1.8$ mm, $\mu_{L_2} = 70$ mm, $\sigma_{L_2} = 7$ mm, $\mu_{L_3} = 60$ mm, $\sigma_{L_3} = 6$ mm; t and R both follow the lognormal distribution, and their ideal distribution parameters are $\mu_t = 1.85$ mm, $\sigma_t = 0.111$ mm, $\mu_R = 4$ mm and $\sigma_R = 0.24$ mm. For a thin-walled beam in an automotive body, the axial impact force (average normal impact force on the rigid wall) is a very important index to evaluate its crashworthiness performance, which is closely related to the occupant security. Thus, in this application, a reliability analysis is conducted for the axial impact force F_{crash} of the beam, and the following limit-state function is created:

$$g\left(L_1, L_2, L_3, t, R\right) = F_a - F_{\text{crash}}\left(L_1, L_2, L_3, t, R\right), \tag{39}$$

where $F_a = 55$ KN denotes an allowable value of the axial impact force.

Table 5 Material properties of the closed-hat beam

Young's Modulus (E)	Poisson's ratio (ν)	Density (ρ)	Yield stress (σ_s)	Tangent modulus (E_t)
2.0×10^5 Mpa	0.27	7.85×10^{-3} Kg/mm^3	310 Mpa	763 Mpa

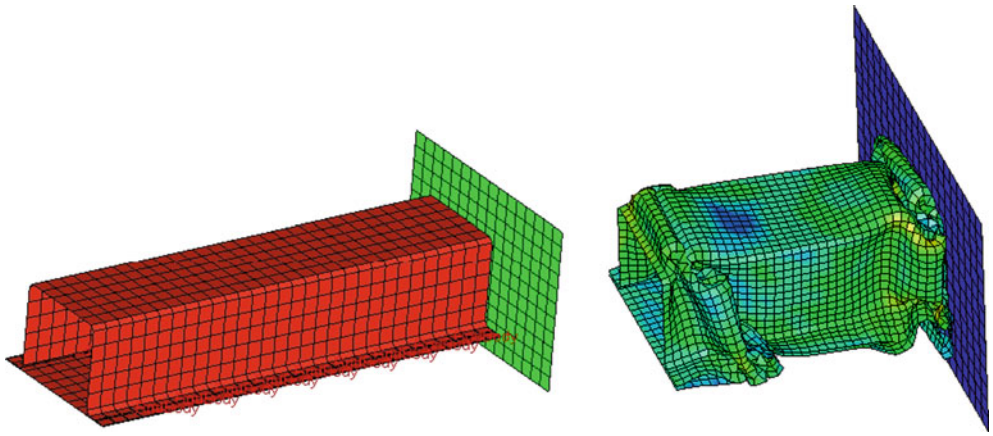

Fig. 15 An FEM model for the impacting process

Table 6 Hybrid reliabilities for crashworthiness performance of a thin-walled beam

C_F	R_H	Convergence point				
		t	R	L_1	L_2	L_3
0.05	0.976	2.011	3.985	18.666	69.729	62.726
0.25	1.294	2.005	3.642	18.942	70.627	63.142

FEM is used to compute the axial impact force, and an elasto-plasticity material model of bilinear kinematic hardening is used with the parameters given in Table 5. The time duration of the impacting process is 20 ms. The Belytschko–Tsay shell element [37] is used to create the FEM mesh of the impacting system as shown in Fig. 15, and the total number of the elements is 4,200. A concentrated mass with a weight of 250 Kg is attached to the end of the closed-hat beam in order to supply enough crushing energy.

Two different cases of $C_F = 0.05$ and $C_F = 0.25$ are considered in this application, and the reliability analysis results are given in Table 6. For $C_F = 0.05$, the reliability of the axial impact force is only 0.976, which actually is not a satisfactory result for crashworthiness performance of a practical automotive body. However, for $C_F = 0.25$, the reliability increases to a relatively large value 1.294, which implies a prominent promotion of the crashworthiness performance. The above analysis once again indicates that through reducing the uncertainty domain the structural reliability can be effectively improved. Thus, in practical applications, we should have a better control of the dimensional deviations of the five uncertain parameters through improving their manufacturing and measuring precision. Through such a treatment, we can obtain a tighter uncertainty domain and thereby a better reliability of the crashworthiness performance of this thin-walled beam.

5 Conclusion

In this paper, a new reliability analysis method is proposed for structures with truncated probability distributions. By using the truncated distributions, a better consistence can be ensured between the random quantification and the practical deviations of the parameters, and hence, the precision of the reliability analysis can be improved by a certain extent. By combining the probability and non-probability analysis techniques, a hybrid reliability model is constructed for the truncated distribution problems. An efficient method is also formulated to compute the hybrid reliability based on a qualitative judgment of the positional relation between the uncertainty domain and the failure surface, which seems effective for most practical engineering problems though it is not so rigorous in mathematics. Three numerical examples with explicit expressions are investigated, and in each one, the truncating ratio of the random parameters is made to change continuously. The computational results show that the hybrid reliability behaves as a continuous and monotonically increasing variation with respect

to the truncating ratio. Furthermore, in the probability analysis stage, the hybrid reliability exhibits a nearly linear relation with the truncating ratio, while a distinctly nonlinear behavior in the non-probability analysis stage. An inflexion point will emerge when the uncertainty domain and the failure surface has only a tangent point. The present method is also applied to a practical engineering problem, namely the reliability analysis of crashworthiness performance for an automotive thin-walled beam. Based on a complex FEM model, the hybrid reliability for the axis impact force of the beam is successfully analyzed under two different cases of the truncating ratio.

Acknowledgments This work is supported by the National Science Foundation of China (11172096), the Key Project of Chinese National Programs for Fundamental Research and Development (2010CB832700) and the program for Century Excellent Talents in University (NCET-11-0124).

References

1. Hasofer, A.M., Lind, N.C.: Exact and invariant second-moment code format. ASME J. Eng. Mech. Div. **100**, 111–121 (1974)
2. Rackwitz, R., Fiessler, B.: Structural reliability under combined random load sequences. Comput. Struct. **9**, 489–494 (1978)
3. Hohenbichler, M., Rackwitz, R.: Non-normal dependent vectors in structural safety. ASME J. Eng. Mech. Div. **107**, 1227–1238 (1981)
4. Breitung, K.W.: Asymptotic approximation for multinormal integrals. ASCE J. Eng. Mech. **110**, 357–366 (1984)
5. Breitung, K.W.: Asymptotic Approximations for Probability Integrals. Springer, Berlin (1994)
6. Polidori, D.C., Beck, J.L., Papadimitriou, C.: New approximations for reliability integrals. ASCE J. Eng. Mech. **125**, 466–475 (1994)
7. Thoft-Christensen, P., Murotsu, Y.: Application of Structural Systems Reliability Theory. Springer, Berlin (1986)
8. Ang, A.H.S., Tang, W.H.: Probability Concepts in Engineering Planning and Design. vol II: Decision, Risk and Reliability. Wiley, New York (1984)
9. Rubinstein, R.Y., Kroese, D.P.: Simulation and The Monte-Carlo Method, 2nd edn. Wiley, New York (2007)
10. Augusti, G., Baratta, A., Gasciati, F.: Probabilistic Methods in Structural Engineering. Chapman and Hall, London (1984)
11. Kirjner-Neto, C., Polak, E., Kiureghian, D.: An outer approximations approach to reliability-based optimal design of structures. J. Optim. Theory Appl. **98**, 1–16 (1998)
12. Royset, J.O., Kiureghian, A.D., Polak, E.: Reliability-based optimal structural design by the decoupling approach. Reliab. Eng. Syst. Saf. **73**, 213–221 (2001)
13. Cheng, G.D., Xu, L., Jiang, L.: A sequential approximate programming strategy for reliability-based structural optimization. Comput. Struct. **84**, 1353–1367 (2006)
14. Liang, J.H., Mourelatos, Z.P., Nikolaidis, E.: A single-loop approach for system reliability-based desing optimization. ASME J. Mech. Des. **129**, 1215–1224 (2007)
15. Luo, Y.J., Kang, Z., Luo, Z., Alex, L.: Continuum topology optimization with non-probabilistic reliability constraints based on multi-ellipsoid convex model. Struct. Multidiscip. Optim. **39**, 297–310 (2008)
16. Kang, Z., Luo, Y.J.: Reliability-based structural optimization with probability and convex set hybrid models. Struct. Multidiscip. Optim. **42**, 89–102 (2010)
17. Du, X.P., Chen, W.: Sequential optimization and reliability assessment method for efficient probabilistic design. ASME J. Mech. Des. **126**, 225–233 (2004)
18. Sweet, A.L., Tu, J.F.: Evaluating tolerances and process capability when using truncated probability density functions. Int. J. Prod. Res. **44**, 3493–3508 (2006)
19. Sun, Z.L., He, X.H.: Reliability calculation method based on cutting-off tail distribution at two ends. Mach. Des. Manuf. **4**, 10–12 (1997)
20. He, S.Q., Wang, S.: Structural Reliability Analysis and Design. National Defence Industry Press, Beijing (1993)
21. Xu, F.Y., Chen, A.R.: Structural reliability analysis based on truncated probabilistic distribution. Eng. Mech. **23**, 52–57 (2006)
22. Melchers, R.E., Ahammed, M., Middleton, C.: FORM for discontinuous and truncated probability density functions. Struct. Saf. **25**, 305–313 (2003)
23. Ben-Haim, Y., Elishakoff, I.: Convex Models of Uncertainties in Applied Mechanics. Elsevier, Amsterdam (1990)
24. Qiu, Z.P., Wang, XJ.: Parameter perturbation method for dynamic responses of structures with uncertain-but-bounded parameters based on interval analysis. Int. J. Solids Struct. **42**, 4958–4970 (2005)
25. Au, F.T.K., Cheng, Y.S., Tham, L.G., Zeng, G.W.: Robust design of structures using convex models. Comput. Struct. **81**, 2611–2619 (2003)
26. Jiang, C., Han, X., Liu, G.R.: Optimization of structures with uncertain constraints based on convex model and satisfaction degree of interval. Comput. Methods Appl. Mech. Eng. **196**, 4791–4890 (2007)
27. Guo, X., Bai, W., Zhang, W.S.: Extremal structural response analysis of truss structures under load uncertainty via SDP relaxation. Comput. Struct. **87**, 246–253 (2009)
28. Ganzerli, S., Pantelides, C.P.: Optimum structural design via convex model superposition. Comput. Struct. **74**, 639–647 (2000)
29. Ganzerli, S., Pantelides, C.P.: Load and resistance convex model for optimum design. J. Struct. Multidiscip. Optim. **17**, 259–268 (1999)
30. Sun, Z.L., Chen, L.Y.: Practical Theory and Method for Mechanical Reliability Design. Science Press, Beijing (2003)
31. Madsen, H.O., Krenk, S., Lind, N.C.: Methods of Structural Safety. Prentice-Hall, Englewood Cliffs (1986)
32. Guo, S.X., Lu, Z.Z., Feng, Y.S.: A non-probabilistic model of structural reliability based on interval analysis. J. Comput. Mech. **18**, 56–60 (2001)

33. Chen, X.Y., Tang, C.Y., Tsui, C.P., Fan, J.P.: Modified scheme based on semi-analytic approach for computing non-probabilistic reliability index. Acta Mech. Solida. Sin. **23**, 115–123 (2010)
34. Yuan, Y.X., Sun, W.Y.: Optimization Theories and Methods. Scientific Press, Beijing (2005)
35. Du, X.P.: Saddlepoint approximation for sequential optimization and reliability analysis. ASME J. Mech. Des. **130**, 011022–0110011 (2008)
36. Jiang, C., Han, X.: A new uncertain optimization method based on intervals and an approximation management model. CMES-Comp. Model. Eng. **22**, 97–118 (2007)
37. Belytschko, T., Liu, W.K., Moran, B.: Nonlinear Finite Elements for Continua and Structures, 3rd edn. Wiley, Chichester (2000)